Published in final edited form as:
J Phys Chem C Nanomater Interfaces. 2011 March 3; 115(8): 3220–3228. doi:10.1021/jp108812z.

On the Binding Strength Sequence for Nucleic Acid Bases and C_{60} with Density Functional and Dispersion-corrected Density Functional Theories: Whether C_{60} could protect nucleic acid bases from radiation-induced damage?

Wenming Sun[†],
The Center for Modeling & Simulation Chemistry, Institute of Theoretical Chemistry, Shandong University, Jinan, 250100, People's Republic of China

Yuxiang Bu[1,†], and
The Center for Modeling & Simulation Chemistry, Institute of Theoretical Chemistry, Shandong University, Jinan, 250100, People's Republic of China

Yixuan Wang[‡]
Department of Natural Science, Albany State University, Albany, Georgia 31705

Abstract

The major objective of this paper is to address a controversial binding sequence between nucleic acid bases (NABs) and C_{60} by investigating adsorptions of NABs and their cations on C_{60} fullerene with a variety of density functional theories including two novel hybrid meta-GGA functionals, M05-2x and M06-2x, as well as a dispersion-corrected density functional, PBE-D. The M05-2x/6-311++G** provides the same binding sequence as previously reported, guanine(G) > cytosine(C) > adenine (A) > thymine (T); however, M06-2x switches the binding strengths of A and C, and PBE-D eventually results in the following sequence, G>A>T>C, which is the same as the widely accepted hierarchy for the stacking of NABs on other carbon nanomaterials such as single-walled carbon nanotube and graphite. The results indicate that the questionable relative binding strength is due to insufficient electron correlation treatment with the M05-2x or even the M06-2x method. The binding energy of G@C_{60} obtained with the M06-2x/6-311++G(d,p) and the PBE-D/cc-pVDZ is −7.10 and −8.07 kcal/mol, respectively, and the latter is only slightly weaker than that predicted by the MP2/6-31G(d,p) (−8.10kca/mol). Thus, the PDE-D performs better than the M06-2x for the observed NAB@C_{60} π-stacked complexes. To discuss whether C_{60} could prevent NABs from radiation-induced damage, ionization potentials of NABs and C_{60}, and frontier molecular orbitals of the complexes NABs@C_{60} and $(NABs@C_{60})^{+}$ are also extensively investigated. These results revealed that when an electron escapes from the complexes, a hole was preferentially created in C_{60} for T and C complexes, while for G and A the hole delocalizes over the entire complex, rather than a localization on the C_{60} moiety. The interesting finding might open a new strategy for protecting DNA from radiation-induced damage and offer a new idea for designing C_{60}-based antiradiation drugs.

[1]The corresponding authors: Yuxiang Bu, byx@sdu.edu.cn; Yixuan Wang, Yixuan.Wang@asurams.edu.
[†]Shandong University
[‡]Albany State University

Supporting Information Available: Figure S1 displays the geometries of various NAB@C_{60} systems obtained at the PW91/DNP level in the gas phase. Table S1 shows the adiabatic and vertical IP calculated with B3LYP/6-31G(d) for the isolated molecules optimized at the PBE-D/cc-pVDZ level. Table S2 summarizes the relative energies (in kcal/mol) of various configurations at the PW91/DNP level. This material is available free of charge via the Internet at http://pubs.acs.org.

Keywords

radiation-induced damage; NAB; C60; dispersion-corrected DFT; binding sequence

1. Introduction

With a rapid development and wide application, the potential effect of nanoparticles on health and environment begins to be a hot topic in the nanotechnology field. A recent issue of *Nano Today* reported that manufacture and use of nanoparticles in medicine and other industries could pose a potential risk to human health.[1] As a typical nanoparticle, since its discovery C_{60} has attracted considerable interest in the field of nanotechnology due to its unique properties. Because of its small size and poor solubility in polar solvents, it may penetrate through cellular membrane, resulting in adverse effects on biological systems, such as traveling through blood stream to heart and depositing on the targeted part of human body causing tissue hurt, lung disease and some toxic effects on human.[2] In spite of potential unfriendly to environment, a good deal of experiments have also established prospective applications for C_{60} derivatives (water-soluble fullerene derivatives) in many fields such as antioxidants, neuroprotective agents, antiapoptotic activity, DNA photocleavage, enzyme inhibition, antimicrobial activity and anti-HIV activity.[3] Various applications of C_{60} derivatives have been reviewed by Nakamura *et al*.[4] Particularly, C_{60} fullerene is proposed to serve as a future antiradiation drug to protect against the side effects of cancer radiation therapy,[5] which is a beneficial effect on biological systems. Understanding about the interaction mechanism between C_{60} or C_{60} derivatives and biomolecules can promote such kind of biomedical applications.

Oxidative DNA damage could cause several diseases, such as cancer[6] and aging[7]. Radiation is one of the most general reasons for oxidative DNA damage.[8] When the high-energy radiation interacts with DNA, an electron may be ejected from DNA, and a hole created in this way migrates over a long distance through a hopping mechanism,[9] eventually ending on a guanine base of DNA because it has the lowest ionization potential among all DNA bases.[10] The guanine radical cation ($G^{\cdot+}$) is a harbinger of many pathological conditions in living cells as a result of its involvement in many multiform reactions.[11] As measured by photoionization yield, the adiabatic IP of C_{60} fullerene molecule is close to 7.54eV,[12] which is lower than the adiabatic IP of guanine (7.77eV), the lowest one among four NABs.[13] This trend is also confirmed by the PBE calculation (Table S1 in the Supporting Information). Consequently, a question is raised whether C_{60} could protect guanine and other DNA bases from radiation-induced damage. Upon a high-energy radiation interacting with NAB@C_{60} complexes, a hole will be created. If the hole localizes on the C_{60} moiety rather than on the NAB moiety, it may demonstrate that C_{60} can act as an antiradiation substance. This investigation is meaningful for the anticipative application of fullerenes in the antiradiation drug field. [5]

To the best of our knowledge, there are few literatures about this issue. Shukla *et al* did useful pioneering research and trials in this topic, and located a stable geometry of C_{60}-guanine.[11a] During the preparation of the paper, another closely relevant paper from Shukla *et al* was released on the website of *Chem. Phys. Lett*.[11b] In the most recent paper, a novel hybrid meta-GGA DFT, M05-2X, was used to reveal the binding strength of NABs and C_{60} molecules. Nevertheless, their binding energies and binding strength sequence may be questionable. The binding strength follows the order: G (−4.99kcal/mol) > C(−4.26) >A (−4.10) > T(−3.75), which is different from the well reported binding strength of DNA bases with single-walled carbon nanotube (SWNT) and graphite, G>A>T>C.[14] In addition, the binding energy of G-C_{60} is quite far from that obtained with MP2 method (−4.99 versus

−8.10 kcal/mol).[11a] Shukla *et al* [11b] claimed that the binding strength order predicted by the M05-2x/6-311++G(d,p) followed a recent experimental report, G>C>A>T. [15] However, the sequence is for poly-nucleotide/SWNT hybrids, specifically, 12-base-long single stranded DNA homopolymers consisting of poly $d(A)_{12}$, poly $d(T)_{12}$, poly $d(C)_{12}$ or poly $d(G)_{12}$, *rather than* for the single DNA base molecules. Because of quite different self-stacking of base molecules in ssDNA, the binding between the ssDNA and SWNT may be different from that of single base and SWNT. On the other hand, even for the poly-nucleotide, a different binding strength measured with spectroscopy is G>A>T>C.[16] Although the HF level together with classical force field[14c] and constraint optimizations with MPWB1K density functional [14a] predicted the binding order of G > A > T > C in the gas phase for the interaction of NABs with (5,5) SWCNT, the binding order based upon isothermal calorimetry experiments on much larger diameter nanotube was predicted to be T > A > C. [14c] The solvent effects may be responsible for the diffidence.

The above deficiencies motivated us to revisit the system with more accurate methods dealing with “long range” electron correlation effects, such as, M06-2x and DFT-D methods. The results will allow us to get insights into whether the above strange strength order originates from the M05-2x method or it really is. As reported by Hobza *et al*,[17] empirical dispersion-corrected density method functional (DFT-D, specifically TPSS-D) provides more accurate results for the π-stacked adenine dimers than M06-2x does. However, Sherrill *et al*’s assessment indicated that M06-2x performs somewhat better than PBE-D for the π-stacked NAB dimers.[18] Thus, in addition to providing a benchmark binding strength for stacked complexes NABs@C_{60}, another objective of the paper is to assess performance of M05-2x, M06-2x and DFD-D on the π-stacked NABs@C_{60}. Furthermore, cationic systems $(NABs@C_{60})^{+}$ were also extensively investigated in order to explore whether fullerenes could protect NABs from radiation-induced damage.

2. Computational Methods

Full geometry optimizations and property calculations for DNA bases and C_{60} were firstly performed with generalized gradient approximation (GGA) type of DFT, PW91 with a double numerical plus polarization function (DNP) basis sets, implemented in DMol^3 package from Accelrys, Inc.[19] The spin polarization scheme was utilized to deal with open-shell systems. The convergence threshold of energy was set as 10^{-7} a.u. Vibrational frequency analysis was also carried out at the level of geometry optimization. The optimized complexes were all minimum energy species along the potential energy surface. The less extensive method aims to extensively search for the π-stacked conformations for complexes NABs@C_{60}.

It is known that, in spite of great improvement over LDA, a typical GGA type of DFT like the above PW91 method still underestimates the binding for the systems mainly arising from van der Waals (vdW) interaction. Hybrid meta-GGA functionals, M05-2X and M06-2x, developed by Truhlar *et al* [20] and implemented in Gaussian 09, [21] better describing the non-bonding interaction than PW91, were therefore also employed to fully optimize a few favorable structures for each NAB.

For an empirical dispersion-corrected density functional theory (DFT-D), Grimme’s scheme was adopted,[22] where the vdw interaction term is well described by a damped interatomic potential, accounting for long-range dispersion effects in noncovalent systems. The total density functional energy can be written as follows:

$$E_{DFT-D}=E_{DFT}+E_{vdw} \quad (1)$$

where E_{DFT} is the normal self-consistent density functional energy, and E_{vdw} is the empirical dispersion correction term and is given by

$$E_{vdw} = -s_6 \sum_{i=i}^{N-1} \sum_{j=i+1}^{N} \frac{C_6^{ij}}{R_{ij}^6} f_{dmp}(R_{ij}) \quad (2)$$

Here, s_6 is a global scaling factor only depending on the applied density functional method.

As usual, the combined dispersion coefficient for atom pair i and j, C_6^{ij}, was estimated with a geometric mean of individual C_6 coefficient, while R_{ij}, the interatomic distance between atoms i and j, is an arithmetic mean value of individual vdw radius. N is the number of atoms, and f_{dmp} (R_{ij}), a damping function, is expressed by the following equation

$$f_{dmp}(R_{ij}) = \frac{1}{1+e^{-\alpha(R/R_0-1)}} \quad (3)$$

Where α is taken to be 20 in the exponent. Perdew-Burke-Ernzerhof (PBE) [23] exchange-correlation functional in the DFT part was employed in the present work, and the DFT-D method was therefore referred to as PBE-D. The PBE-D calculations were conducted with the ORCA suite of programs.[24] Dunning's correlation-consistent polarized valence basis sets of double-zeta (cc-pVDZ) and/or triple-zeta (cc-pVTZ) were used together with the PBE-D method, as usually applied to the other π-π stacking systems.[18] All of the relevant systems were also fully optimized at the PBE-D levels.

3. Results and Discussion

3.1. Neutral Complexes (NABs@C_{60}) in the Gas Phase

With the PW91/DNP method, a variety of positions of NABs over C_{60} were investigated. In C_{60} fullerene, the *hh* C-C bond (the C-C bond shared by two hexagonal rings) has more π-bonding character than the *hp* C-C bond (the C-C bond shared by a hexagonal ring and a pentagonal ring).[25] There are three distinct symmetry sites in C_{60} with respect to the hexagonal ring in NAB molecules: bridge, top and hollow. The adsorption on hollow site is less stable than on the other two sites. The hollow conformation therefore will not be discussed below. Various geometries and the relative energies at the PW91/DNP level are shown in Figure S1 and Table S2 in the Supporting Information.

For thymine (T), guanine (G), and cytosine (C), adsorption on the bridge site is the most stable, while for adenine the most stable one is on the top site. The fullerene molecule in these complexes does not undergo significant deformation. The binding energy E_b for the neutral complexes NAB@C_{60} is defined as:

$$E_b = E(\text{NAB@C}_{60}) - E(\text{NAB}) - E(\text{C}_{60}) \quad (4)$$

where E(NAB-C_{60}), E(C_{60}), and E(NAB) are the total energies for the complex, isolated C_{60}, and NAB, respectively. It was widely accepted that the BSSE effect is nearly negligible when the numerical basis sets are employed.[19] The basis set superposition error (BSSE) was therefore not included for the PW91/DNP level with Dmol^3 code, and however, it was taken into account with counterpoise scheme at the M05-2x, M06-2x and PBE-D levels.[26]

As shown in Table 1, the binding energies from the PW91/DNP for NAB@C_{60} are quite small. Obviously, all NABs undergo physisorption processes when they interact with C_{60}. G@C_{60} complex has the strongest binding (−2.63 kcal/mol), followed by C-C_{60} (−2.30 kcal/mol) and A-C_{60} (−2.12 kcal/mol), and T-C_{60} complex has the lowest binding energy (−1.78 kcal/mol). This binding trend, G > C > A > T, is the same as that predicted by Shukla *et al* with M05-2X/6-311++G(d, p), although the binding is dramatically weaker than that obtained by M05-2X/6-311++G(d, p). The present full optimization with the M05-2x method generates the same binding energies for G@C_{60} and C@C_{60} complexes as reported by Shukla *et al*,[11b] and those for T@C_{60} and A@C_{60} only slightly differ (−3.70 and −4.16 kcal/mol versus −3.75 and −4.10 kcal/mol). Although their detailed geometries for the NBA@C60 complexes are not available, because of rather similar binding energies the geometries from the present and Shukla's work should be very similar as well. Except for the similar one for G@C_{60} (3.031Å in the present work versus 3.041Å) the nearest distances between heavy (non-hydrogen) atom of NABs and carbon atoms of C_{60} differ by 0.1–0.2Å different (3.001, 2.993, and 3.131Å versus 3.249, 3.245, and 3.220Å), which may arise from different definitions.

Table 1 also shows that both the M06-2x/cc-pVDZ and M06-2x/6-311++G(d,p) significantly enhance the binding between NABs and C_{60} by 1–2 kcal/mol as compared with those from the M05-2x/6-311++G(d,p). It is interesting to note that the relative binding strength for C@C_{60} and A@C_{60} is opposite to that obtained by the M05-2X/6-311++G(d,p). The binding sequence for NBAs@C_{60} is consequently changed to G>A>C>T. Although M06-2x is considerably improved in describing the non-covalent interaction over other GGAs,[20] there is still some deficiency compared with the dispersion-corrected density methods (DFT-D).[17] As compared with the results from the M06-2x, the present PBE-D/cc-pVDZ does further strengthen the binding between NABs and C_{60} so that the BSSE-corrected binding energy for G@C_{60} complex (−8.07kcal/mol) is only slightly less negative than −8.10kcal/mol, obtained at the MP2/6-31G(d,p)//MP2/6-31G(d) level.[11a] Thus, for the examined π-stacked dimers NAB@C_{60}, it seems that PDE-D performs better than M06 does. Since it is well known the MP2 method overestimates non-covalent interaction to some extent, the results obtained by PBE-D/cc-PVDZ method may be rather close to the real values of the binding energies. The PBE-D turns out that the binding strength between NABs@C_{60} follows the sequence: G > A >T >C, which is the same as the binding sequence of NABs with (5, 5) as well as (10, 0) SWNTs [14a, 14c] and the hierarchy of NABs with a graphene layer as well as graphite surface.[14d, 27] PBE-D/cc-PVTZ further enhances the binding of NABs with C_{60} by approximately 0.1kcal/mol for A, C, and T, yet by 0.35 kcal/mol for G. However, the binding strength remains the same as that from the PBE-D/cc-pVDZ. A variation of the binding strength for NABs@C_{60} with theoretical methods is shown in Figure 2.

The displaced-stacked π-π interaction between NABs and C_{60} is stabilized mainly by dispersion effect depending on the surface area of buried as well as on the polarizability of the moieties.[28] Since there are both five-membered imidazole ring and six-membered pyrimidine ring in guanine and adenine molecules, the π-π stacking interactions between adenine/guanine and C_{60} should be generally stronger than thymine/cytosine with one only six-membered ring. London's empirical formula may help understand the above binding sequence for the NABs@C_{60} complexes. [29]

$$E_{AB}^{disp} = -\frac{3\alpha^A \alpha^B I_A I_B}{4(I_A + I_B)R^6} \quad (5)$$

where α and I are the polarizability and ionization potential for individual molecules, respectively, and R is the distance between molecules A and B. The polarizability of NABs, representing the deformability of the electronic charge distribution, is known to arise from the regions associated with the aromatic rings, lone electron pairs in nitrogen, and oxygen atoms. Guanine has the largest value of polarizability (120.8 au at the B3LYP/6-31G(d) level), followed by adenine (108.6 au), and thymine and cytosine have similar ones (94.7 and 90.5 au). This trend is the same as Gowtham's report.[27] Based on London's equation, the ratio of the dispersion forces of the four complexes is approximately as, 100% (G@C_{60}): 89%(A@C_{60}): 81%(T@C_{60}): 75%(C@C_{60}), which also supports that A@C_{60} and T@C_{60} should be stronger than C@C_{60}. Especially, the prediction confirms the binding sequence obtained by the PBE-D method.

To gain further insights into the electronic structures, Figure 3 illustrates the highest occupied molecular orbitals (HOMO) and the lowest unoccupied molecular orbitals (LUMO) of these complexes. LUMO of all these complexes localizes on C_{60}. Orbital energies for the HOMO of the five individual molecules are as follows: G(−0.208 a.u.) > A(−0.218)> C_{60} (−0.220) > C(−0.227) > T(−0.240). As shown by the molecular orbitals in Figure 3 and the energy level diagrams in Figure 4, HOMOs from the NAB and C_{60} make different contributions to the HOMO of complexes. For G@C_{60} and A@C_{60}, the HOMO levels of the complexes are close to the HOMO of NAB, while the HOMO levels of complexes C@C_{60} and T@C_{60} are close to the HOMO level of C_{60}. According to Figure 3, HOMOs delocalize over both guanine/adenine moiety and C_{60} for G/A@C_{60} complexes, while they almost localize on C_{60} in T/C@C_{60} complexes. Accordingly, the presence of C_{60} molecule may well protect thymine and cytosine from radiation damage. However, whether fullerene could protect guanine and adenine from radiation damage needs to be further investigated.

3.2. Cationic Complexes (NABs@C_{60})$^+$ in the Gas Phase

For the four (NABs@C_{60})$^+$ complexes (NAB=A, C, G and T), both the π-π stacked and the T-shaped σ-π conformations were optimized with the PW91/DNP, M05-2x/cc-pVDZ, M06-2x/cc-pVDZ, M06-2x/6-311++G**, and PBE-D/cc-pVDZ methods. The first ionization potentials of NAB and C_{60} from the theoretical methods were summarized in Table 3 together with the experimental data. The M06-2x, PBE-D, and MPWB1K predicted that C_{60} has lower adiabatic IP than T, C and A, yet higher aIP than G. At the M06-2x/cc-pVDZ level the aIPs for the NABs are lower by 0.1–0.2eV than the experimental data, while the M06-2x/6-311++G** yields higher ones by 0.1–2eV. Thus, because of higher aIP than C_{60} for the ionic complexes of A, C, and T with C_{60} the binding energy was defined for (NABs@C_{60})$^+$ as:

$$E_b^+ = E(\mathrm{NAB@C_{60}})^+ - E(\mathrm{NAB}) - E(\mathrm{C_{60}})^+ \quad (6a)$$

Because of lower aIP than C_{60} for the ionic complexes of G with C_{60},

$$E_b^+ = E(\mathrm{NAB@C_{60}})^+ - E(\mathrm{C_{60}}) - E(\mathrm{NAB})^+ \quad (6b)$$

The superscript "+" represents the cationic system, the other notations are the same as them in equation (4). In the cationic complexes, because of the predictable electrostatic force, the binding energies listed in Table 2 are higher negative than those of the neutral complexes NAB@C_{60}. Figure 5 shows the π-stacked as well as the T-shaped σ-π conformations for the complexes (NAB@C_{60})$^+$, together with the nearest distances. For the π-stacked

conformations, consistent with stronger binding the nearest distances for the cationic complexes are shorter than those for the neutral counterparts, e.g., at the PBE-D/cc-pVDZ level, 2.805, 2.351, 2.812 and 3.034 Å versus 2.974, 3.129, 2.913 and 3.125 Å for adenine, cytosine, guanine, and thymine, respectively.

At the PW91/DNP level, except for the π-stacked geometry of $(A@C_{60})^+$ that still maintains the favorable conformation similar to its neutral complex, for the other three complexes C_{60}^+ binds with NABs through π and carbonyl oxygen, referred to as σ-π conformation. When electron correlation effects are well taken into account by the M05-2x, M06-2x and PBE-D methods, the located conformations are significant different from those obtained with the PW91/DNP method. At the M05-2x/cc-pVDZ level, for $(C@C_{60})^+$ the initial π-stacked conformations always converge to the σ-π conformation, while for other three cationic complexes $(NAB@C_{60})^+$ both the π-π stacked and T-shaped σ-π conformations were located. The stacked $(T@C_{60})^+$ is only 0.8 kcal/mol less stable than the T-shaped one. According to Table 2, however, the π-stacked conformation is more stable than the σ-π one by 6.7 and 6.0 kcal/mol for the $(A@C_{60})^+$ and $(G@C_{60})^+$ complexes, respectively.

As shown in Figure 5, as electron correlation is better included by the M06-2x/cc-pVDZ and M06-2x/6-311++G** methods, a rather tilted stacked conformation for $(C@C_{60})^+$ was also predicted, but it is considerably less stable than the T-shaped σ-π conformation by 14.5 and 10.8 kcal/mol. At the PBE-D/cc-pVDZ level, although the stacked conformation for $(C@C_{60})^+$ is still less stable than the T-shaped one, their binding energy difference is just 4.8 kcal/mol. The M06-2x/cc-pVDZ, M06-2x/6-311++G**, and PBE-D/cc-pVDZ also switch the relative binding for the $(T@C_{60})^+$ predicted by the M05-2x, e.g., the stacking is stronger than the σ-π interaction by approximately 1–2 kcal/mol. At the PBE/cc-pVDZ level, the binding strength including BSSE corrections decrease in the sequence, G (−22.7kcal/mol)> C(−20.3) >A(−19.0) >T (−13.6).

Obviously, favorable geometries of the cationic complexes are very sensitive to the applied theoretical methods. For the $(NBAs@C_{60})^+$ complexes, two principal forces, dispersion and electrostatic force, may determine the conformations of $(NBAs@C_{60})^+$. Because of possessing two aromatic rings, guanine and adenine interact more strongly with C_{60}^+ via dispersion force than one-ring cytosine and thymine. When the high level methods are applied, such as M06-2x and PBE-D that can accurately deal with electron correlation inducing dispersion force, for adenine and guanine the favorable conformations are therefore the π-stacked ones. On the other hand, because of the positively charged surface in C_{60}^+, electrostatic force in $(NBAs@C_{60})^+$ plays more important role on determining the conformation than in the neutral complexes. The unique oxygen atom in cytosine carries more negative charge (−0.362e) than carbonyl oxygen atoms (−0.338 and −0.354e) in thymine. The stronger electrostatic interaction between the oxygen of cytosine and C_{60}^+ induces a favorable T-shaped σ-π conformation for $(C@C_{60})^+$ complex. Actually, as shown in Table 2 and Figure 5 only M06-2x and PBE-D predicts a rather tilted partially stacked conformation that is less stable than the T-shaped $(C@C_{60})^+$. For the $(T@C_{60})^+$ complex, the two major driving forces are well balanced, and both the stacked and T-shaped conformations are brought about at the M05-2x, M06-2x and PBE-D levels. Since the PW91 considerably underestimates dispersion force, at this level electrostatic force may determine the optimal complexes. Thus, for $(C@C_{60})^+$, $(G@C_{60})^+$, and $(T@C_{60})^+$ complexes the conformations obtained by PW91/DNP are T-shaped, which also supports the claim that the T-shaped configuration has more stabilizing electrostatic interaction than the displaced π-π stacking configuration due to favorable quadrupole-quadrupole interaction.[30]

3.3 Hole Distribution and Its Biological Implication

To address the other objective whether fullerene can protect DNA bases from radiation damage, the spin densities for $(NBAs@C_{60})^+$ were illustrated in Figure 6 together with the atomic charge fitted from electrostatic potential and the total spin density on the C_{60} moiety. The total atomic charges on the C_{60} are +0.632e, +0.731e, +0.850e and +0.863e for the π-stacked $(G@C_{60})^+$, $(A@C_{60})^+$, $(T@C_{60})^+$, and $(C@C_{60})^+$, respectively, while for the T-shaped $(C@C_{60})^+$ and $(T@C_{60})^+$ the charges are even larger (+0.888e and +0.975e). This shows that an electron can be dominantly ejected from the C_{60} moiety for the $(C@C_{60})$ and $(T@C_{60})$ complexes upon photoionization or radiation. As a result, the trapped hole also mainly distributes over the C_{60} portion in $(C@C_{60})^+$ and $(T@C_{60})^+$, which is further supported by the high spin density in the C_{60} moiety ranging from 0.764 for the π-stacked $(T@C_{60})^+$ to 0.924 for the T-shaped $(T@C_{60})^+$. The above significant spin density localization over the C_{60} moiety in the $(C@C_{60})^+$ and $(T@C_{60})^+$ complexes demonstrates that the presence of C_{60} could well prevent C and T from radiation or photoionization. The spin density on the C_{60} of $(A@C_{60})^+$ is lower than those of the π-stacked $(C@C_{60})^+$ and $(T@C_{60})^+$ by approximately 0.1, (0.670 versus 0.849 and 0.760). For $(G@C_{60})^+$, the spin density almost equivalently delocalizes over guanine and C_{60} (0.461 versus 0.539). Thus, C_{60} could only partially protect A and G from radiation damage by sharing the injected hole.

The above spin density distribution scenario somehow agrees well with the IP difference between C_{60} and NABs. The lager the IP difference, the higher the degree of the spin density delocalization over C_{60}. To obtain a more remarkable performance for NABs protection, it is therefore suggested to synthesize and utilize new fullerene derivatives that have a significant IP gap with guanine.

IP values for the complexes were also calculated, as defined below,

$$\mathrm{IP}(\mathrm{NAB@C_{60}}) = E(\mathrm{NAB@C_{60}})^+ - E(\mathrm{NAB@C_{60}}) \quad (7)$$

Combination of equations (4), (6) and (7), results in,

$$\mathrm{IP}(\mathrm{NAB@C_{60}}) = (E_b^+ - E_b) + \mathrm{IP}(\mathrm{C_{60}}) \quad (8)$$

Binding energies of the cationic systems (E_b^+) are much more negative than their corresponding neutral systems (E_b). Thus, IP of the complex is smaller than C_{60} as well as NABs. As shown in Figure 7, the discrepancies between IPs of four NAB@C_{60} complexes are smaller than those of four NABs. These observations indicate that the binding of NABs with C_{60} can reduce the IP of whole system by sharing the hole as possible, leading NAB@C_{60} to promising hole carriers or relays for the long-range charge migration. Further, the trend of IPs for NAB@C_{60} is also different from that for the isolated NAB molecules. For the NAB@C_{60} complexes, A@C_{60} has larger IP than C@C_{60}, which is opposite to the isolated NAB (IP(C) > IP(A)). G@C_{60} still has the lowest IP in the four complexes just as guanine in the four NABs. This implies that the NAB@C_{60} carriers or relays of a hole are property-tunable via varying the base partners of C_{60}.

Clearly, all above predictions are derived from the steady-state analysis on the properties of the NAB@C_{60} complexes. However, some dynamics information are still unknown which hopefully provide the dynamic knowledge for a deep understanding of the interaction of the shortly-separated NABs and C_{60} and their charge transfers. In addition, the protein surroundings and solvent molecules may yield considerable effects on the interaction modes

between NABs and C_{60}, the charge transfer mechanism among them, and tunability of the carrier/relay properties of the NAB@C_{60} complexes. Further investigations are certainly needed for a clarification of all these details.

4. Conclusions

In summary, geometric and electronic properties of NAB@C_{60} and $(NAB@C_{60})^+$ were extensively investigated by the M05-2x, M06-2x and PBE-D methods. The binding strength sequence for the neutral complex NAB@C_{60} varies with the applied theoretical methods. The M05-2x/6-311++G** provides the same binding sequence as previously reported by Shukla et al.,[11b] guanine (G) > cytosine (C) > adenine (A) > thymine (T); however, the binding strengths of A and C are switched at the M06-2x level, resulting in the binding sequence, G > A > C > T. When dispersion force is explicitly included by the PBE-D method, the above sequence is further revised to, G>A>T>C, which is the same as the binding sequence of NABs with SWNTs, a graphene layer as well as a graphite surface,[14a, 14c–d, 27] and also follows the sequence predicted by the London's dispersion equation. The results indicate that the previous questionable relative binding strength is due to insufficient electron correlation treatment with the M05-2x. A comparison among the predicted binding energy with different methods for G@C_{60} shows that PDE-D performs better than M06-2x. At both the M06-2x and PBE-D levels, the favorable conformation for $(A@C_{60})^+$, $(G@C_{60})^+$, and $(T@C_{60})^+$ is the π-stacked one; while for $(C@C_{60})^+$ the T-shaped σ-π conformation is more favorable. The frontier molecular orbital analysis reveals that when an electron escapes from the complexes, the hole dominantly localizes on C_{60} for $(C@C_{60})^+$ and $(T@C_{60})^+$, while for $(A@C_{60})^+$ and $(G@C_{60})^+$ delocalizes over the entire complex. Thus, the presence of C_{60} may well prevent C and T from radiation damage, while only partially protect A and G. It should be noted that protein surrounding and solvent effect could modify the binding modes and even the charge distributions, thus providing a possibility in regulating the interactions and charge exchange mechanism between the NABs and C_{60} and competition among four NAB bases. This work is being expanded with great efforts in our co-laboratory.

Supplementary Material

Refer to Web version on PubMed Central for supplementary material.

Acknowledgments

This work at Shandong University (Sun and Bu) is supported by NSFC (20633060, 20973101), NCET, and the Independent Innovation Foundation (2009JC020) of Shandong University. The project described here was also supported in part by the National Institute of General Medical of the National Institute of Health (SC3GM082324), the American Recovery and Reinvestment Act (3SC3GM082324-02S1) and ACS PRF (47286-GB5) in terms of scholarly development (Wang at Albany State University). We are also grateful to Dr. Zhengfeng Xu for optimizing the complexes $(NAB@C_{60})^+$ at M06-2x/6-311++G(d,p) level.

References

1. Sealy C. Nanoparticles cause DNA damage, according to new reports. Nano Today. 2010; 5(1):1.
2. Nel A, Xia T, Madler L, Li N. Toxic Potential of Materials at the Nanolevel. Science. 2006; 311(5761):622–627. [PubMed: 16456071]
3. Bosi S, Da Ros T, Spalluto G, Prato M. Fullerene derivatives: an attractive tool for biological applications. Euro J Med Chem. 2003; 38(11–12):913–923.
4. Nakamura E, Isobe H. Functionalized Fullerenes in Water. The First 10 Years of Their Chemistry, Biology, and Nanoscience. Acc Chem Res. 2003; 36(11):807–815. [PubMed: 14622027]

5. Bhatia A. Nuclear Medicine In 21st Millennium: An Approach Via Nanotechnology. Asian J Exp Sci. 2008; 22(2):12.
6. Loft S, Poulsen HE. Cancer risk and oxidative DNA damage in man. J Mol Med. 1996; 74(6):297–312. [PubMed: 8862511]
7. Mecocci P, Fanó G, Fulle S, MacGarvey U, Shinobu L, Polidori MC, Cherubini A, Vecchiet J, Senin U, Beal MF. Age-dependent increases in oxidative damage to DNA, lipids, and proteins in human skeletal muscle. Free Rad Bio Med. 1999; 26(3–4):303–308. [PubMed: 9895220]
8. Burrows CJ, Muller JG. Oxidative Nucleobase Modifications Leading to Strand Scission. Chem Rev. 1998; 98(3):1109–1152. [PubMed: 11848927]
9. Giese B, Amaudrut J, Kohler AK, Spormann M, Wessely S. Direct observation of hole transfer through DNA by hopping between adenine bases and by tunnelling. Nature. 2001; 412(6844):318–320. [PubMed: 11460159]
10. Steenken S. Purine bases, nucleosides, and nucleotides: aqueous solution redox chemistry and transformation reactions of their radical cations and e- and OH adducts. Chem Rev. 1989; 89(3): 503–520.
11. (a) Shukla MK, Leszczynski J. Fullerene (C60) forms stable complex with nucleic acid base guanine. Chem Phys Lett. 2009; 469(1–3):207–209. (b) Shukla MK, Dubey M, Zakar E, Namburu R, Leszczynski J. Interaction of nucleic acid bases and Watson-Crick base pairs with fullerene: Computational study. Chem Phys Lett. 2010; 493(1–3):130–134.
12. Hertel IV, Steger H, de Vries J, Weisser B, Menzel C, Kamke B, Kamke W. Giant plasmon excitation in free C_{60} and C_{70} molecules studied by photoionization. Phys Rev Lett. 1992; 68:784. [PubMed: 10045992]
13. Orlov VM, Smirnov AN, Varshavsky YM. Ionization potentials and electron-donor ability of nucleic acid babes and their analogues. Tetra Lett. 1976; 17(48):4377–4378.
14. (a) Wang Y. Theoretical Evidence for the Stronger Ability of Thymine to Disperse SWCNT than Cytosine and Adenine: Self-Stacking of DNA Bases vs Their Cross-Stacking with SWCNT. J Phys Chem C. 2008; 112(37):14297–14305. (b) Wang YX, Bu YX. Noncovalent Interactions between Cytosine and SWCNT: Curvature Dependence of Complexes via π•••π Stacking and Cooperative CH•••π/NH•••π. J Phys Chem B. 2007; 111:6520–6526. [PubMed: 17508735] (c) Das A, Sood AK, Maiti PK, Das M, Varadarajan R, Rao CNR. Binding of nucleobases with single-walled carbon nanotubes: Theory and experiment. Chem Phys Lett. 2008; 453(4–6):266–273. (d) Sowerby SJ, Cohn CA, Heck WM, Holm NG. Differential adsorption of nucleic acid bases: Relevance to the origin of life. Proc Natl Acad Sci. 2001; 98:3. [PubMed: 11136240]
15. Albertorio F, Hughes ME, Golovchenko JA, Branton D. Base dependent DNA-carbon nanotube interactions: activation enthalpies and assembly-disassembly control. Nanotech. 2009:20.
16. Manohar S, Mantz AR, Bancroft KE, Hui C-Y, Jagota A, Vezenov DV. Peeling single-stranded DNA from graphite surface to determine oligonucleotide binding energy by force spectroscopy. Nano Lett. 2008; 8:8.
17. Morgado CA, Jurecka P, Svozil D, Hobza P, Sponer J. Reference MP2/CBS and CCSD(T) quantum-chemical calculations on stacked adenine dimers. Comparison with DFT-D, MP2.5, SCS(MI)-MP2, M06-2X, CBS(SCS-D) and force field descriptions. Phys Chem Chem Phys. 2010; 12:3522. [PubMed: 20336251]
18. Sherrill, CDT Tait; Hohenstein, Edward G. An Assessment of Theoretical Methods for Nonbonded Interactions: Comparison to Complete Basis Set Limit Coupled-Cluster Potential Energy Curves for the Benzene Dimer, the Methane Dimer, Benzene-Methane, and Benzene-H2S. J Phys Chem A. 2009; 113:10146–10159. [PubMed: 19689152]
19. (a) Delley B. An all-electron numerical method for solving the local density functional for polyatomic molecules. J Chem Phys. 1990; 92(1):508–517. (b) Delley B. From molecules to solids with the DMol[sup 3] approach. J Chem Phys. 2000; 113(18):7756–7764.
20. Zhao Y, Schultz NE, Truhlar DG. Design of Density Functionals by Combining the Method of Constraint Satisfaction with Parametrization for Thermochemistry, Thermochemical Kinetics, and Noncovalent Interactions. J Chem Theory Comput. 2006; 2(2):364–382.
21. Frisch, MJ.; Trucks, GW.; Schlegel, HB.; Scuseria, GE.; Robb, MA.; Cheeseman, JR.; Scalmani, G.; Barone, V.; Mennucci, B.; Petersson, GA.; Nakatsuji, H.; Caricato, M.; Li, X.; Hratchian, HP.;

Izmaylov, AF.; Bloino, J.; Zheng, G.; Sonnenberg, JL.; Hada, M.; Ehara, M.; Toyota, K.; Fukuda, R.; Hasegawa, J.; Ishida, M.; Nakajima, T.; Honda, Y.; Kitao, O.; Nakai, H.; Vreven, T.; Montgomery, JA., Jr; JEP; Ogliaro, F.; Bearpark, M.; Heyd, JJ.; Brothers, E.; Kudin, KN.; Staroverov, VN.; Kobayashi, R.; Normand, J.; Raghavachari, K.; Rendell, A.; Burant, JC.; Iyengar, SS.; Tomasi, J.; Cossi, M.; Rega, N.; Millam, JM.; Klene, M.; Knox, JE.; Cross, JB.; Bakken, V.; Adamo, C.; Jaramillo, J.; Gomperts, R.; Stratmann, RE.; Yazyev, O.; Austin, AJ.; Cammi, R.; Pomelli, C.; Ochterski, JW.; Martin, RL.; Morokuma, K.; Zakrzewski, VG.; Voth, GA.; Salvador, P.; Dannenberg, JJ.; Dapprich, S.; Daniels, AD.; Farkas, O.; Foresman, JB.; Ortiz, JV.; Cioslowski, J.; Fox, DJ. Gaussian 09, Revision A.02. Gaussian, Inc; Pittsburgh PA: 2009.

22. (a) Grimme S. Accurate description of van der Waals complexes by density functional theory including empirical corrections. J Comput Chem. 2004; 25(12):1463–1473. [PubMed: 15224390] (b) Grimme S. Semiempirical GGA-type density functional constructed with a long-range dispersion correction. J Comput Chem. 2006; 27(15):1787–1799. [PubMed: 16955487]
23. Perdew JP, Burke K, Ernzerhof M. Generalized Gradient Approximation Made Simple. Phys Rev Lett. 1996; 77(18):3865. [PubMed: 10062328]
24. Neese, F. ORCA-an ab initio, density functional and semiempirical program package, Ver. 2.8.0. Max-Planck-Institut fur Bioanorganische Chemie; Mulheim an der Ruhr: 2010.
25. Wu X, Zeng XC. First-Principles Study of a Carbon Nanobud. ACS Nano. 2008; 2(7):1459–1465. [PubMed: 19206315]
26. Boys SF, Bernardi F. The calculation of small molecular interactions by the differences of separate total energies. Some procedures with reduced errors. Mol Phys. 1970; 19(4):553–566.
27. Gowtham S, Scheicher RH, Ahuja R, Pandey R, Karna SP. Physisorption of nucleobases on graphene: Density-functional calculations. Phys Rev B. 2007; 76(3):033401.
28. Guckian KM, Schweitzer BA, Ren RXF, Sheils CJ, Tahmassebi DC, Kool ET. Factors Contributing to Aromatic Stacking in Water: Evaluation in the Context of DNA. J Am Chem Soc. 2000; 122(10):2213–2222. [PubMed: 20865137]
29. London F. Zur Theorie und Systematik der Molekularkräfte. Zeitschrift für Physik A Hadrons and Nuclei. 1930; 63(3):245–279.
30. Sinnokrot MO, Sherrill CD. Highly Accurate Coupled Cluster Potential Energy Curves for the Benzene Dimer: Sandwich, T-Shaped, and Parallel-Displaced Configurations. J Phys Chem A. 2004; 108(46):10200–10207.
31. Lias SG, Bartmess JE, Liebman JF, Holmes JL, Levin RD, Mallard WG. Gas-phase ion and neutral thermochemistry. J Phys Chem Ref Data, supplement. 1988; 17:1.

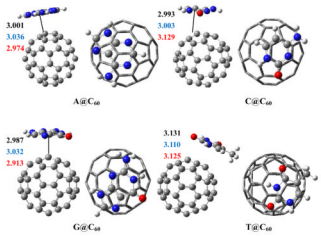

Figure 1. Side- and top views of π-stacked NAB@C_{60} complexes

The dark, blue and red data are the nearest distance between non-hydrogen atom of NBA and C_{60} with the M05-2x/6-311++G(d,p), M06-2x/6-311++G(d,p) and PBE-D/cc-pVDZ methods, respectively.

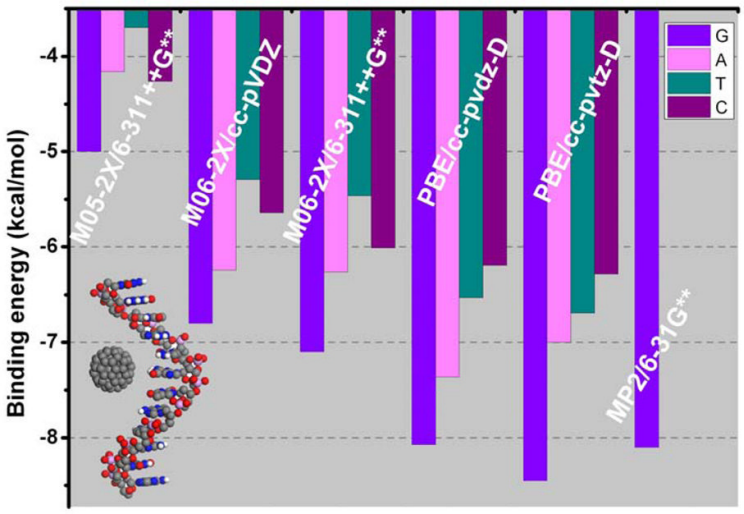

Figure 2.
Variation of binding strength for (NAB@C_{60}) with theoretical methods.

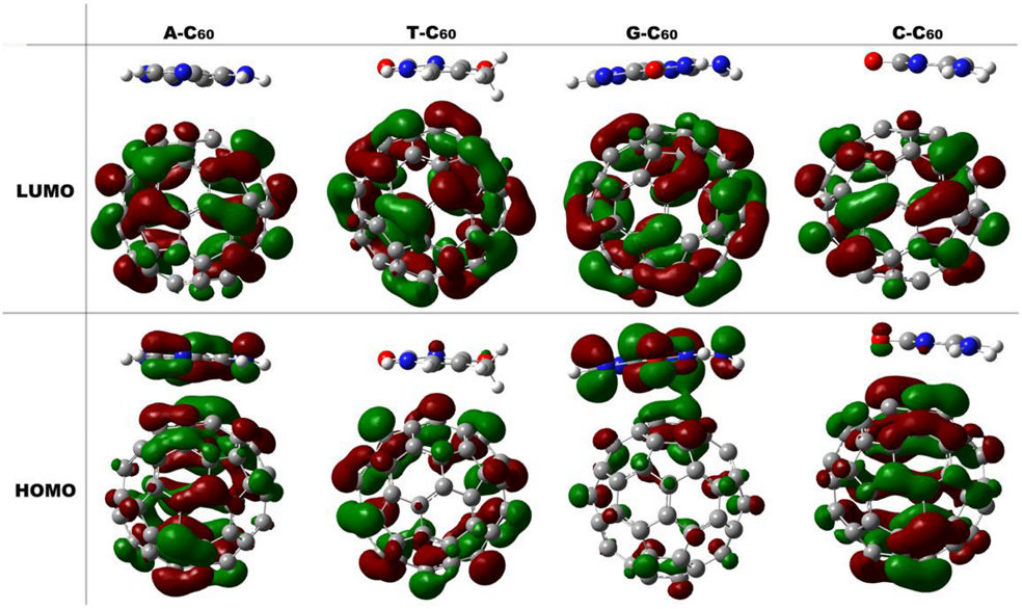

Figure 3.
Plots of the frontier orbitals of the NAB@C_{60} complexes. The isovalue is 0.02 a.u.

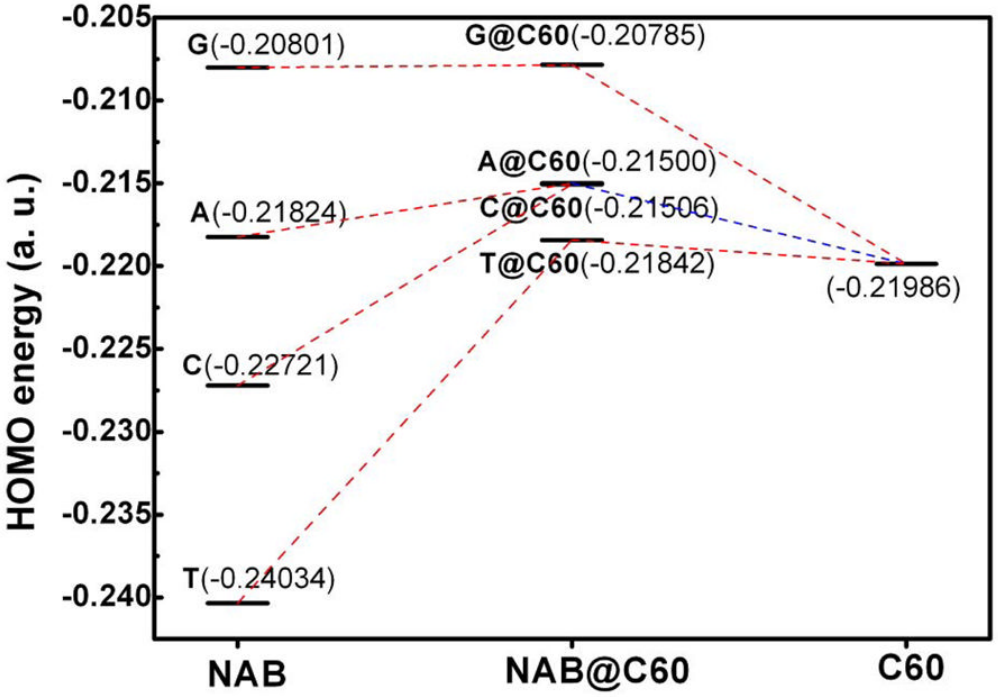

Figure 4.

Molecular orbital energy level diagrams (au). The LUMO levels of NABs are significant higher than C_{60}. LUMO of NABs therefore has no contribution to the LUMO of complexes. For clarity NABs' LUMO level are not shown in this picture. HOMO energies of A@C60 and C@C60 are too close to distinguish.

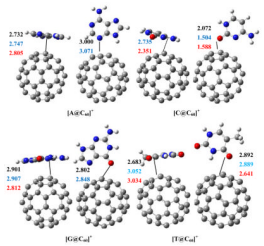

Figure 5. π-stacked and T-shaped $[NAB@C_{60}]^+$ complexes

The dark, blue and red data are the nearest distance between non-hydrogen atom of NBA and C_{60} with M05-2x/cc-PVDZ, M06-2x/cc-PVDZ, and PBE-D/cc-pVDZ methods, respectively.

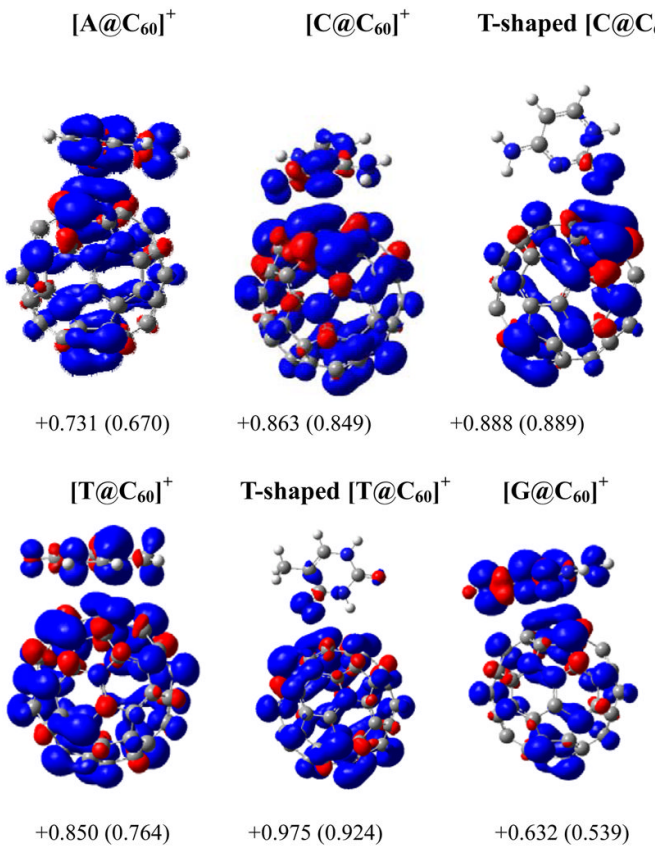

Figure 6.

The spin density surface of cationic complexes $(NABs@C_{60})^+$ with an isovalue of 0.004au. The numbers below each panel stand for the charge from ESP fitting and total spin density (in parentheses) in C_{60} moiety.

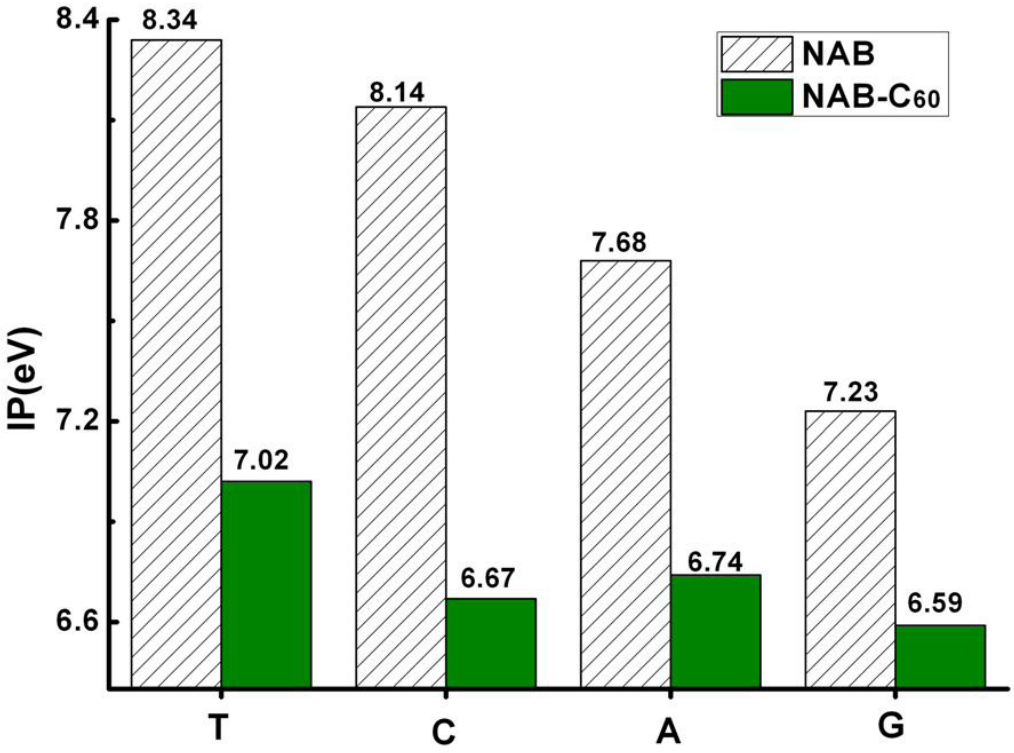

Figure 7.
Adiabatic IP values of the individual NABs and NABs@C_{60} complexes in the gas phase at the PBE-D/cc-pVDZ level, while that of C_{60} is 7.25eV.

Table 1

Binding energies (kcal/mol) for the neutral complexes with the PW91, M05, M06 and PBE-D methods. Basis sets A, B, and C are cc-pVDZ, 6-311++G(d,p), and cc-pVTZ, respectively.

Complex	PW91/DNP	M052x/A	M052x/B	M052x/B[a]	M062x/A	M062x/B[b]	PBE-D/A	PBE-D/C
A@C_{60}	−2.12	−4.06	−4.16	−4.10	−6.24	−6.26(−6.40)	−7.36	−7.42
C@C_{60}	−2.30	−3.78	−4.26	−4.26	−5.64	−6.01(−6.07)	−6.19	−6.34
G@C_{60}	−2.63	−4.67	−5.00	−4.99	−6.80	−7.10(−7.55)	−8.07	−8.45 −8.10[c]
T@C_{60}	−1.78	−3.54	−3.70	−3.75	−5.29	−5.46(−5.56)	−6.53	−6.69

[a] Ref. 11b;

[b] The data in parenthesis are those without deformation correction;

[c] Ref. 11a.

Table 2

Binding energies (kcal/mol) for $(NAB@C_{60})^+$ at various calculation levels.

Complexes		PW91/DNP	M05-2x/cc-pVDZ	M06-2x/cc-pVDZ[a]	M06-2x/6-311++G**	PBE-D/cc-pVDZ[a]
$(A@C_{60})^+$	stacking	−11.1	−16.4	−17.6 (−14.3)	−15.7	−22.2(−19.0)
$(A@C_{60})^+$	σ-π	—	−9.7	−10.7	−7.1	—
$(C@C_{60})^+$	stacking	—	—	−15.4	−14.5	−22.0(−17.6)
$(C@C_{60})^+$	σ-π	−14.4	−31.5	−29.9 (−24.1)	−25.3	−26.8(−20.3)
$(G@C_{60})^+$	stacking	—	−12.8	−14.5	−16.5	−26.1(−22.70)
$(G@C_{60})^+$	σ-π	−18.7	−6.8	−10.7	−14.2	—
$(T@C_{60})^+$	stacking	—	−8.3	−11.0	−11.2	−15.9(−13.5)
$(T@C_{60})^+$	σ-π	−9.4	−9.1	−9.7	−9.7	−13.2(−10.6)

[a]The data in parentheses include BSSE correction.

J Phys Chem C Nanomater Interfaces. Author manuscript; available in PMC 2011 May 25.

Table 3

The first adiabatic and vertical ionization potentials (aIP and vIP/eV) for nucleic acid bases and C_{60} at various theoretical levels.

	Thymine	Cytosine	Adenine	Guanine	C_{60}
aIP, M052x/cc-pVDZ	8.73	8.59	8.02	7.56	8.04
aIP, M062x/cc-pVDZ	8.71	8.58	8.02	7.56	7.96
aIP, M062x/6-311++G**	8.97	8.90	8.31	7.87	8.03
aIP, PBE-D/cc-pVDZ	8.34	8.14	7.68	7.23	7.25
vIP, PBE-D/cc-pVDZ	8.47	8.29	7.89	7.54	7.31
aIP, MPWB1K/cc-pVDZ	8.62	8.38	7.88	7.38	7.68
aIP, Exp.[a/b]	8.87/8.80	8.68/8.45	8.26/7.80	7.77/7.85	
IP, Experimental range[c]					7.54–8.1

[a] Photoionization mass spectroscopy in the gas phase. [13];

[b] Photoelectron spectra. [31]

[c] Ionization energy determinations for C_{60} at chemistry web book of NIST

J Phys Chem C Nanomater Interfaces. Author manuscript; available in PMC 2011 May 25.